arXiv:1603.03375v3 [cond-mat.supr-con] 28 Oct 2016

Beyond Triplet: Unconventional Superconductivity in a Spin-3/2 Topological Semimetal

Hyunsoo Kim,[1,2,3,*] Kefeng Wang,[1,2] Yasuyuki Nakajima,[1,2] Rongwei Hu,[1,2] Steven Ziemak,[1,2] Paul Syers,[1,2] Limin Wang,[1,2] Halyna Hodovanets,[1,2] Jonathan D. Denlinger,[4] Philip M. R. Brydon,[5,6] Daniel F. Agterberg,[7] Makariy A. Tanatar,[3] Ruslan Prozorov,[3] and Johnpierre Paglione[1,2,†]

[1] *Center for Nanophysics and Advanced Materials, University of Maryland, College Park, MD 20742, USA*
[2] *Department of Physics, University of Maryland, College Park, MD 20742, USA*
[3] *Ames Laboratory, Department of Physics & Astronomy, Iowa State University, Ames 50011, USA*
[4] *Advanced Light Source, Lawrence Berkeley National Laboratory, Berkeley, CA 94720, USA*
[5] *Condensed Matter Theory Center and Joint Quantum Institute, Department of Physics, University of Maryland, College Park, MD 20742, USA*
[6] *Department of Physics, University of Otago, P.O. Box 56, Dunedin 9054, New Zealand*
[7] *Department of Physics, University of Wisconsin, Milwaukee, WI, USA*

(Dated: October 31, 2016)

In all known fermionic superfluids, Cooper pairs are composed of spin-1/2 quasi-particles that pair to form either spin-singlet or spin-triplet bound states. The "spin" of a Bloch electron, however, is fixed by the symmetries of the crystal and the atomic orbitals from which it is derived, and in some cases can behave as if it were a spin-3/2 particle. The superconducting state of such a system allows pairing beyond spin-triplet, with higher spin quasi-particles combining to form quintet or even septet pairs. Here, we report evidence of unconventional superconductivity emerging from a spin-3/2 quasiparticle electronic structure in the half-Heusler semimetal YPtBi, a low-carrier density noncentrosymmetric cubic material with a high symmetry that preserves the p-like $j = 3/2$ manifold in the Bi-based Γ_8 band in the presence of strong spin-orbit coupling. With a striking linear temperature dependence of the London penetration depth, the existence of line nodes in the superconducting order parameter Δ is directly explained by a mixed-parity Cooper pairing model with high total angular momentum, consistent with a high-spin fermionic superfluid state. We propose a $\mathbf{k} \cdot \mathbf{p}$ model of the $j = 3/2$ fermions to explain how a dominant J=3 septet pairing state is the simplest solution that naturally produces nodes in the mixed even-odd parity gap. Together with the underlying topologically non-trivial band structure, the unconventional pairing in this system represents a truly novel form of superfluidity that has strong potential for leading the development of a new generation of topological superconductors.

When spin-orbit coupling is strong enough to rearrange the order of electronic energy bands, various topological phases arise, and the interplay between superconductivity and the topologically ordered phase is of particular interest [1, 2]. The noncentrosymmetric half-Heusler compounds containing heavy metallic elements exhibit a strong spin-orbit coupling which can invert the Bi-derived s-like Γ_6 and p-like Γ_8 bands, giving a semimetal system with non-trivial topological electronic structure [3–5]. The observation of superconductivity in the RPtBi [6–11] and and RPdBi series [11] (where R=rare earth) has added a new richness to these materials that compounds topological aspects of normal state band structure, superconductivity and even magnetic order [12]. In the superconducting state wavefunction, non-trivial topologies can arise both in fully gapped superconductors [13] and unconventional superconductors with point or line nodes, in particular in Weyl and noncentrosymmetric superconductors [14]. In the latter, the lack of parity symmetry can lead to mixed even-odd parity pairing states on spin-split Fermi surfaces due to antisymmetric spin-orbit coupling [15, 16].

The situation in these materials is further enriched by the j=3/2 total angular momentum index of the states in the Γ_8 electronic band near the chemical potential. This arises from the strong atomic spin-orbit coupling of the s=1/2 spin and the l=1 orbital angular momenta in the p atomic states of Bi. The high crystal symmetry and the relatively simple band structure conspire to preserve the j=3/2 character of the low-energy electronic states, permitting Cooper pairs with angular momentum beyond the usual spin-singlet or spin-triplet states. In particular, as demonstrated schematically in Fig. 1, high angular momentum even- and odd-parity pairing components with quintet ($J = 2$) and septet ($J = 3$) states are possible through the pairing combinations of spin-1/2 and spin-3/2 quasiparticles, giving rise to the possibility of the high-spin superfluidity usually discussed in the context of fermionic cold atoms [17, 18], but realized in the solid state. Such an unprecedented exotic pairing state arises from new j=3/2 interactions that do not appear for the spin-1/2 case, allowing new opportunities for topological superconducting states [19].

Here we focus on the archetype topological half-Heusler YPtBi, a clean limit superconductor with an extremely small electronic density of states $N(0)$ at the

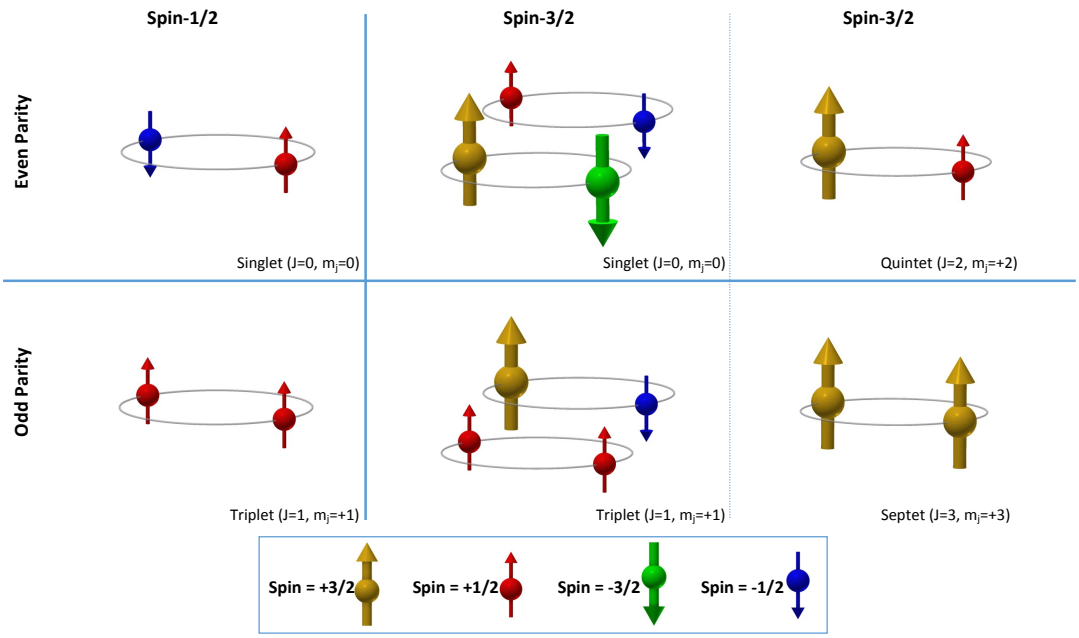

FIG. 1. **High-spin Cooper pairing.** In conventional spin 1/2 systems, there exists four pairing channels among the spin $-1/2$ and $1/2$ states: one spin singlet (with total angular momentum given by $J = 0$ and with the z component of angular momentum, J_z given by $m_J = 0$) and three spin-triplet, with $J = 1$ and $m_J = -1, 0, 1$. The Pauli exclusion principle requires the anti-symmetric even valued J states to have even spatial parity and the symmetric odd valued J states to have odd spatial parity. The spin-singlet $J = 0, m_J = 0$ Cooper pair is depicted in panel (a), while the spin-triplet $J = 1, m_J = 1$ Cooper pair is depicted in panel (b). For spin 3/2 systems, there exist sixteen pairing channels among the spin $-3/2$, $-1/2$, $1/2$ and $3/2$ states: one spin-singlet with $J = 0$ and $m_J = 0$, three spin-triplet with $J = 1$ and $m_J = -1, 0, 1$, five spin-quintet with $J = 2$ and $m_J = -2, -1, 0, 1, 2$, and seven spin-septet with $J = 3$ and $m_J = -3, -2, -1, 0, 1, 2, 3$ (see SI for complete listing). The highest m_J state for each J is depicted in panels (c)-(f). In panel (c), the $J = 0, m_J = 0$ spin-singlet pair is a quantum superposition of two Cooper pairs, one pair made from spins $-1/2$ and $1/2$, and the other pair made from spins $-3/2$ and $3/2$. In panel (d), the $J = 1, m_J = 1$ spin-triplet pair is a quantum superposition of two Cooper pairs, one made from two paired spin 1/2 states, and the other from pairing spin 3/2 with spin $-1/2$. Panels (e) and (f) show the $J = 2, m_J = 2$ and $J = 3, m_J = 3$ states, respectively.

Fermi level [20], corresponding to a tiny carrier density $n \approx 2\times10^{18}$ cm^{-3} [7] that rivals that of the record-holder $SrTiO_3$ [21]. The superconducting phase transition at $T_c = 0.78$ K [7] cannot be explained within the BCS theory framework, which would require a carrier density nearly three orders of magnitude larger to explain the critical temperature [22], and the upper critical field $H_{c2}(0) = 1.5$ T exceeds the orbital pair-breaking limit for a conventional s-wave pairing state [7, 23]. In fact, the linear temperature-dependence of the upper critical field over the entire superconducting temperature range [7, 23] resembles that seen in the topological superconductors such as $Cu_xBi_2Se_3$ [24] and Bi_2Se_3 under pressure [25]. Furthermore, point contact spectroscopy measurements in the superconducting state exhibit several anomalous aspects (see SI for details). First, a very large energy gap of 0.2-0.3 meV, also observed in scanning tunneling spectroscopy experiments [26], corresponds to at least twice the BCS expectation of $\Delta_0 = 1.76k_BT_c = 0.1$ meV for a fully gapped superconductor with $T_c = 0.8$ K. Second, a sharp, non-Andreev-like peak of conductance centered at zero bias lies in contrast to the typical split-peak flattened enhancement observed in s-wave superconductors [27], and is very reminiscent of the odd-parity state in Sr_2RuO_4 [28].

To establish a proper pairing model for YPtBi, understanding the electronic structure is essential. Generally, the crystal electric field in a cubic crystal structure splits the degenerate atomic energy levels into two-and six-fold degenerate energy levels at Γ-point as shown in Fig. 2(a) left. Including the strong atomic spin-orbit coupling of Bi partially lifts the degeneracy of the p-derived states, splitting them into the two-fold degenerate Γ_7 and four-fold degenerate Γ_8 bands. In YPtBi, the atomic spin-orbit coupling is sufficiently strong to invert the order of the bands, pushing the s-orbital-derived Γ_6 band below the p-like Γ_8 band. This produces a topological semimetal where the low-energy states have spin-3/2 character.

In order to characterize the band structure, we employ density functional theory (DFT) calculations and angle-resolved photoemission spectroscopy (ARPES) measurements. The calculated bands near the Fermi level along

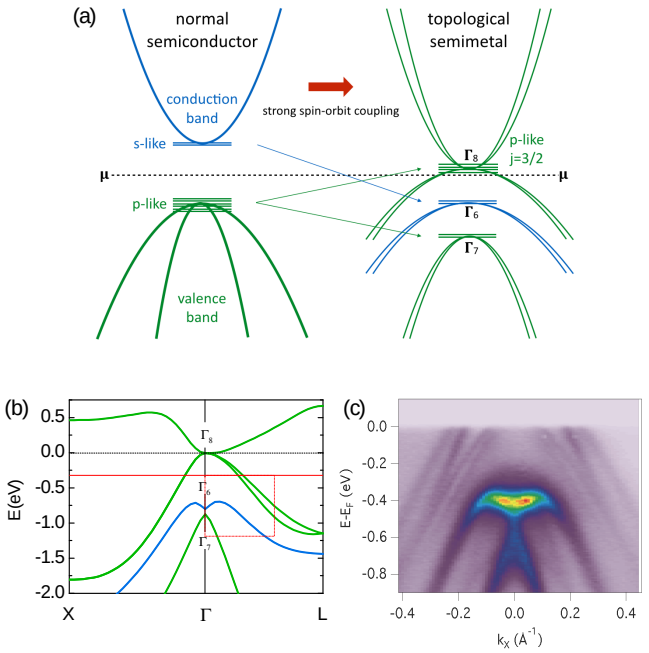

FIG. 2. **Topological p-like states and YPtBi band structure** The effect of strong spin-orbit coupling on a normal semiconductor band structure acts to produce a topological semimetal which retains spin-3/2 character of the original p-like band. As shown schematically in panel (a), as spin-orbit coupling is increased, the s-like conduction band is pushed below the chemical potential μ while the six-fold-degenerate p-like valence band at the Γ-point splits into a two-fold-degenerate Γ_7 band and a four-fold-degenerate Γ_8 conduction band. The absence of parity symmetry in the YPtBi crystal structure generally causes a further splitting of the bands away from the Γ point. Due to the high symmetry of the cubic crystal structure of the half-Heusler material YPtBi, its MBJLDA electronic structure (see text), shown in panel (b), retains the four-fold degeneracy of the p-like j=3/2 states at the Γ-point. Dashed and solid horizontal lines represent E_F determined by calculation and by angle-resolved photoemission spectroscopy, respectively. The band structure was confirmed by ARPES measurements of the valence band dispersions. Panel (c) shows an expanded view of the near-E_F bands at the Γ-point zone center corresponding to the calculated band structure in the dotted rectangle in panel (b). The spectra were measured at $h\nu$=86 eV, which cuts close to the (111)-oriented Brillouin zone center at normal emission. While the outermost pair of bands exhibit 2D-like behavior, the smaller spin-split hole band exhibits a stronger modulation of ARPES intensity, consistent with a bulk-assignment of this inner spin-split hole-band.

the high symmetry points (X-Γ-L) are shown in Fig. 2(b), confirming the topological band inversion of s-like Γ_6 and p-like Γ_8 bands as shown previously [31, 32]. A maximum splitting of the valence hole-band is observed along [111] (Γ-L) and zero-splitting degeneracy along [100] (Γ-X). More extensive theoretical band structure can be found in the SI section.

For experimental verification of the band structure, ARPES experiments focused on spin-split bands across the Fermi energy level. An expanded view of the normal emission zone-center bands, shown in Fig. 2(c), reveals four hole-like E_F-band crossings suggestive of a pair of spin-split bands. While the outermost pair of bands exhibit 2D-like behavior, the smaller spin-split hole band exhibits a stronger modulation of ARPES intensity around the 86 eV bulk Γ-point, consistent with a bulk-assignment of this inner spin-split hole-band. A characteristic Rashba-like splitting of two hole bands are revealed at ≈ 0.5 eV binding energy which also appear in bulk band structure calculations, but at an energy of ≈ -0.8 eV below E_F. With the chemical potential shifted to -0.32 eV, ARPES results show reasonable agreement with the theoretical results (see SI section for details). Based on this observation, the resulting theoretical spin-split Fermi surfaces consist of slightly warped either inward or outward spheres with the degenerate points along (Γ-X) directions.

To determine the spin-splitting of the bulk Fermi surface, the angle-dependent Shubnikov-de Haas (SdH) effect were studied. First, we examine the magnetoresistance derivative, dR_{xx}/dB, in order to access directly to the oscillatory component (actual magnetoresistance data R_{xx} are shown in SI section). Figure 3(a) shows dR_{xx}/dB vs. B at various in-plane angles θ defined from crystallographic [010] direction, measured at 2 K. A beating frequency node-like feature, observable near 7 T for $\theta = 0°$, moves in magnetic field as the angle increases away from the highest symmetry direction. The frequency spectrum of SdH oscillations at θ=90° at various temperatures are shown in Fig. 3(b). Two frequencies of 39 T and 49 T are clearly resolved in the data for $\theta = 0°$, which correspond respectively to the inner and outer spin-split Fermi surfaces. The temperature dependent amplitude of these frequencies was used to determine the representative effective mass m^*=0.11m_e by using Lifshitz-Kosevich theory for both bands. The split peaks are no longer visible above 10 K due to thermal broadening of the corresponding Landau levels.

The most interesting aspect of the band inversion and the experimental position of the chemical potential in the Γ_8 band arises due to the $j = 3/2$ total angular momentum, which comes from spin-orbit coupling of spin $s = 1/2$ electrons in the $l = 1$ p-orbitals of Bi. Near the Fermi energy, we model the Γ_8 bands by a $j = 3/2$ $\mathbf{k}\cdot\mathbf{p}$ theory [33]. Up to quadratic order in k, the single-particle Hamiltonian is

$$H = \alpha k^2 + \beta \sum_i k_i^2 \check{J}_i^2 + \gamma \sum_{i\neq j} k_i k_j \check{J}_i \check{J}_j + \delta \sum_i k_i (\check{J}_{i+1}\check{J}_i\check{J}_{i+1} - \check{J}_{i+2}\check{J}_i\check{J}_{i+2}), \quad (1)$$

where $i = x, y, z$ and $i + 1 = y$ if $i = x$, *etc.*, and $\check{J}_i$ are 4×4 matrix representations of the $j = 3/2$ angu-

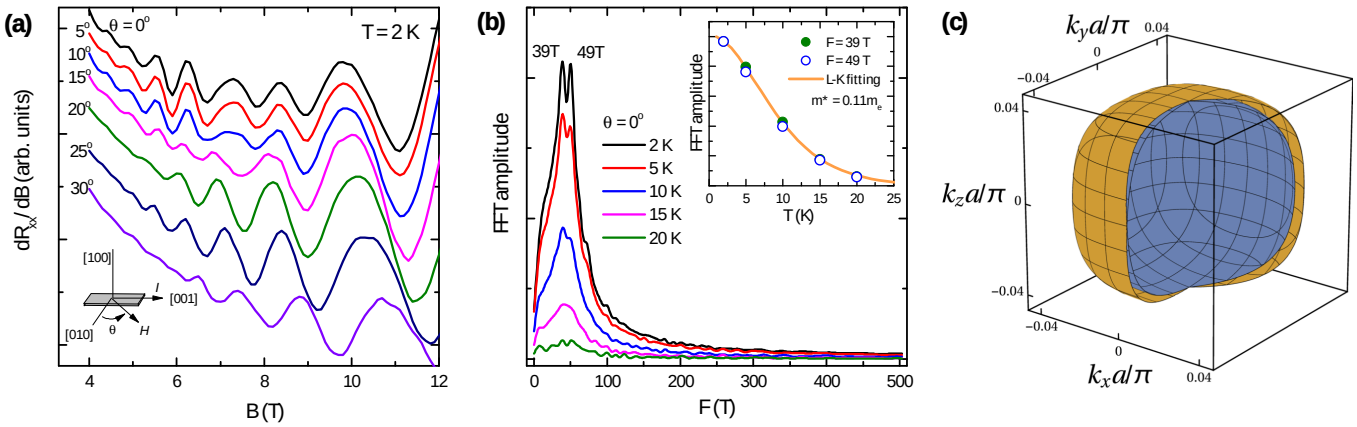

FIG. 3. **Spin-split Fermi surfaces of YPtBi.** Angle-dependent Shubnikov-de Haas oscillations were used to demonstrate the geometry of the spin-split Fermi surfaces. (a) dR_{xx}/dB vs. B at various in-plane angles θ defined from crystallographic [010] direction, measured at 2 K. A node of beating oscillation is observable near 7 T for $\theta = 0°$, moves up in magnetic field as polar angle is increased away from the high symmetry direction, either in positive or negative directions. We plot the magnetoresistance derivative, dR_{xx}/dH, to extract the oscillatory component (actual magnetoresistance data R_{xx} are shown in SI section). (b) Fast Fourier transform spectrum of SdH oscillations at $\theta = 0°$ in various temperatures. The beating frequencies are resolved to be 39 T and 49 T, which correspond respectively to the inner and outer spin-split Fermi surfaces. The temperature dependent amplitude of the FFT spectra is nearly identical for both spin-split Fermi surfaces, and a representative effective mass m^*=0.11m_e was determined by employing the Lifshitz-Kosevich theory to both Fermi surfaces. (c) Theoretical spin-split Fermi surfaces obtained by fitting the $j = 3/2$ $\mathbf{k}\cdot\mathbf{p}$ theory in Eq. (1) to the *ab initio* results by fixing the chemical potential at $\mu = -35$ meV (see text).

lar momentum operators. The first line of Eq. (1) is the Luttinger-Kohn model, while the second line is the antisymmetric SOC due to the broken inversion symmetry in YPtBi. The parameters α, β, γ, and δ are chosen by fitting to our *ab initio* calculations adjusted against ARPES results, which yields $\alpha = 20.5$ eVa^2/π^2, $\beta = -18.5$ eVa^2/π^2, $\gamma = -12.7$ eVa^2/π^2, and $\delta = 0.06eVa/\pi$ by fixing the chemical potential at $\mu = -35$ meV, where a is the lattice constant taken from Ref. [34]. The observed low density of hole carriers is consistent with a Fermi energy lying close to the top of the hole bands, yielding typical Fermi surfaces shown in Fig. 3(c).

The Hamiltonian Eq. (1) has two major implications for the superconductivity in YPtBi. Firstly, since the quasiparticles in the Γ_8 band have intrinsic angular momentum $j = 3/2$, they can form Cooper pairs with higher intrinsic angular momentum than allowed in the conventional theory of $j = 1/2$ quasiparticle pairing; specifically, in addition to the familiar singlet ($J = 0$) and triplet ($J = 1$) states, we must also consider quintet ($J = 2$) and septet ($J = 3$) pairing (see SI for full set of states). Secondly, the absence of inversion symmetry (manifested by the antisymmetric spin-orbit coupling) implies that a stable superconducting state will be dominated by pairing between quasiparticles in time-reversed states near the Fermi energy [15]. As detailed in the supplemental material, this condition is generically satisfied by a mixture of conventional s-wave singlet pairing with an unconventional p-wave septet pairing state [19]. This state is discussed in more detail below and cannot occur for Cooper pairs formed using the usual j=1/2 states.

To further constrain the pairing model, we employ measurements of the temperature-dependent London penetration depth $\Delta\lambda(T)$, which is intimately related to the superconducting order parameter Δ [35]. This approach is particularly useful in the case of YPtBi, where thermodynamic signatures of the superconducting state are difficult to measure, since λ^2 is inversely proportional to $N(0)$. In fact, the absolute value of the zero-temperature $\lambda(0)$ is 1.6 μm [23], about two orders of magnitude greater than that found in conventional superconductors with $T_c \sim 1$ K, such as zinc or aluminum. As show in Fig. 4(a), a sharp transition at $T_c \approx 0.8$ is observed to be consistent with transport measurements [7, 23].

We compare the low-temperature behavior of $\Delta\lambda(T)$ in YPtBi to that of KFe_2As_2 [29], an unconventional superconductor with line nodes [29], and the anisotropic s-wave superconductor $CaPd_2As_2$ [30], both taken using an identical experimental setup. The contrast is striking, with $\Delta\lambda(T)$ in YPtBi being nearly identical to that of KFe_2As_2 and completely different from that of $CaPd_2As_2$. In a fully-gapped s-wave superconductor, the thermally activated quasiparticles are responsible for the expected exponential temperature dependence of $\Delta\lambda(T)$ at low temperatures (see SI for details), while power laws are clear signatures of nodes or zeroes in the superconducting order parameter [35]. In a gap structure with line nodes, the penetration depth varies linearly with temperature at sufficiently low temperatures ($T < 0.3T_c$) in a

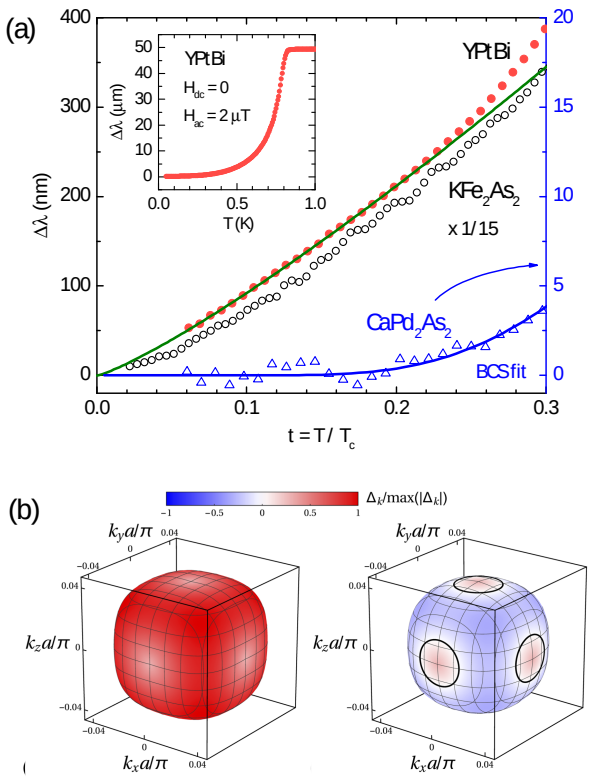

FIG. 4. **Evidence for line nodes and spin-3/2 singlet-septet mixed parity pairing model.** The London penetration depth $\Delta\lambda(T)$ of YPtBi (solid circles) measured in zero dc field (2 μT ac field) is compared in panel (a) with that of KFe_2As_2 (open circles; T_c = 3.4 K), an unconventional superconductor with line nodes [29], and the anisotropic s-wave superconductor $CaPd_2As_2$ (open triangles; T_c = 1.3 K) [30], both taken using an identical experimental setup. The nearly linear variation of $\Delta\lambda(T)$ is in contrast with the isotropic gap dependence (blue line) of the BCS superconductor $CaPd_2As_2$ data, constraining any possible pairing model to one that yields line nodes. Due to the high intrinsic angular momentum of the Γ_8 band quasiparticles involved in Cooper pairing in YPtBi, our $j = 3/2$ $\mathbf{k}\cdot\mathbf{p}$ model yields a manifold of possible pairing states with intrinsic angular momenta up to $J = 3$. Incorporating the lack of inversion symmetry, the singlet-septet pairing state is the simplest even-odd parity mixture with line nodes in the pairing gap that arise from the dominant $J = 3$ septet component. The gap sign and magnitudes are depicted in panel (b) for the two spin-dependent Fermi surfaces of YPtBi, showing the presence of line of zero-gap nodes (black lines) situated on one of the spin-dependent surfaces.

clean sample [36] (see SI for details), such as observed in the prototypical d-wave superconductor $YBa_2Cu_3O_{6.95}$ (YBCO) [37], as well as the mixed-parity noncentrosymmetric superconductors $CePt_3Si$ [38] and Li_2Pt_3B [39].

In YPtBi, $\Delta\lambda(T)$ is best fit to a power-law function $\Delta\lambda = AT^n$ with $n = 1.20 \pm 0.02$ and $A = 1.98 \pm 0.08$ μm/K$^{1.2}$ in a temperature range that spans above $0.2T_c$. This nearly T-linear behavior is consistent with the expectation for a line-nodal superconductor. The observed small deviation from linearity is likely due to moderate impurity scattering, quantified by modifying the temperature dependence $\Delta\lambda(T) = bT^2/(T + T^*)$ [40] with scattering rate parameter $T^* = 0.07T_c$, indicating an exceptionally clean sample. The extraordinarily large power-law pre-factor A in YPtBi is consistent with the London theory expectation $\lambda(0) \propto n^{-2}$ given the small carrier density of this material.

Line nodes can in principle arise from a large number of different pairing states. However, the cubic symmetry of YPtBi imposes severe constraints on the pairing: for example, the pure d-wave state realized in YBCO is very unlikely here, as it would be difficult to avoid mixing with another degenerate d-wave state. Although symmetry permits line nodes due to an extended s-wave state, this requires significant fine-tuning due to the small, nearly spherical Fermi surface of the material. The simplest, most generic model for a nodal order parameter in YPtBi is provided by a mixture of a dominant J=3 (septet) p-wave gap with a subdominant J=0 (singlet) s-wave gap, as allowed by the noncentrosymmetric crystal structure.

As shown in Fig. 4(b), the gap structure resulting from this mixed singlet-septet state displays ring-shape line nodes on one of the spin-split Fermi surfaces. These line nodes are protected by a topological winding number and lead to nondegenerate surface zero-energy flat bands (see SI) [14], which are of immense interest in the context of topological excitations. The mixed singlet-septet state is a natural generalization of the theory of j=1/2 noncentrosymmetric superconductors. As discussed further in the SI, however, the observation of gap line nodes and the broken inversion symmetry may be consistent with other exotic pairing states [17]. Furthermore, with a conventional Eliashberg theory unapplicable to such a low carrier density system, one must consider other pairing instabilities such as parity fluctuations [41, 42] as possible mechanisms of superconductivity in the half-Heusler system. Studying the pairing mechanism of these exotic high angular momentum pairing states, as well as their interplay with other symmetry-breaking orders [11], will elucidate the complexity and richness of this family of multi-faceted topological materials.

METHODS

YPtBi single crystals were grown out of molten Bi with the starting composition Y:Pt:Bi = 1:1:20 (atomic ratio). The starting materials Y ingot (99.5%), Pt powder (99.95%) and Bi chunk (99.999%) were put into an alumina crucible, and the crucible was sealed inside an evacuated quartz ampule. The ampule was heated slowly to 1150°C, kept for 10 hours, and then cooled down to 500°C at a 3°C/hour rate where the excess of molten Bi

was decanted by centrifugation.

The temperature variation of London penetration depth $\Delta\lambda(T)$ was measured in a commercial Kelvinox MX400 dilution refrigerator by using a precise tunnel diode resonator (TDR) technique. The single-crystal sample with dimensions (0.29×0.69×0.24) mm^3 was mounted on a sapphire rod and inserted into a 2 mm inner diameter copper coil that produces rf excitation field with empty-resonator frequency of 22 MHz with amplitude $H_{ac} \approx 2$ μT. The shift of the resonant frequency (in cgs units), $\Delta f(T) = -G4\pi\chi(T)$, where $\chi(T)$ is the differential magnetic susceptibility, $G = f_0 V_s/2V_c(1-N)$ is a constant, N is the demagnetization factor, V_s is the sample volume and V_c is the coil volume. The constant G was determined from the full frequency change by physically pulling the sample out of the coil. With the characteristic sample size, R, $4\pi\chi = (\lambda/R)\tanh(R/\lambda) - 1$, from which $\Delta\lambda$ can be obtained [35].

Angle-resolved photoemission measurements were performed on cleaved single crystals that tend to reveal small regions of (111)-oriented surfaces suitable for observation of sharp bands. Measurements were performed at the MERLIN Beamline 4.0.3 at the Advanced Light Source in the photon energy ($h\nu$) range of 30-150 eV, using a Scienta R8000 hemispherical electron energy analyzer with energy resolution set to ≈ 20 meV, and with the sample cooled to ≈ 30 K in a vacuum of better than 5×10^{-11} Torr.

Magnetic field-dependent magnetoresistance was determined on samples by using a standard four-probe technique. Contacts were made by using high purity silver wires and conducting epoxy, and measurements were performed in a commercial cryostat with a single-axis rotator in magnetic fields up to 14 T at temperatures as low as 2 K.

Acknowledgements

The authors gratefully acknowledge V. Yakovenko and M. Weinert for stimulating discussion. Research at the University of Maryland was supported by Department of Energy (DOE) Early Career Award No. DE-SC-0010605 (experimental investigations) and the Gordon and Betty Moore Foundations EPiQS Initiative through Grant No. GBMF4419 (materials synthesis). Work in Ames was supported by the U.S. DOE Office of Science, Basic Energy Sciences, Materials Science and Engineering Division. Ames Laboratory is operated for the U.S. DOE by Iowa State University under Contract No. DE-AC02-07CH11358. We acknowledge support from Microsoft Station Q, LPS-CMTC, and JQI-NSF-PFC (P.M.R.B), and the NSF via DMREF-1335215 (D.F.A.). ARPES experiments were supported by the U.S. DOE at the Advanced Light Source (DE-AC02-05CH11231).

SUPPLEMENTARY INFORMATION

Spin-3/2 pairing

In YPtBi, the electronic Γ_8 representation responsible for the states near the chemical potential can be described by a $j = 3/2$ basis with four basis elements: $\{|\frac{3}{2}\rangle, |\frac{1}{2}\rangle, |-\frac{1}{2}\rangle, |-\frac{1}{2}\rangle\}$. Physically this basis stems from $l = 1$ p-states coupled to $s = 1/2$ spin. In this direct product space, the basis elements can be expressed as:

$$|\tfrac{3}{2}\rangle = \tfrac{1}{\sqrt{2}}[-|p_x, \tfrac{1}{2}\rangle - i|p_y, \tfrac{1}{2}\rangle] \quad (2)$$

$$|\tfrac{1}{2}\rangle = \tfrac{1}{\sqrt{6}}[2|p_z, \tfrac{1}{2}\rangle - |p_x, -\tfrac{1}{2}\rangle - i|p_y, -\tfrac{1}{2}\rangle] \quad (3)$$

$$|-\tfrac{1}{2}\rangle = \tfrac{1}{\sqrt{6}}[2|p_z, -\tfrac{1}{2}\rangle + |p_x, \tfrac{1}{2}\rangle - i|p_y, \tfrac{1}{2}\rangle] \quad (4)$$

$$|-\tfrac{3}{2}\rangle = \tfrac{1}{\sqrt{2}}[|p_x, -\tfrac{1}{2}\rangle - i|p_y, -\tfrac{1}{2}\rangle]. \quad (5)$$

Cooper pairs can be constructed from these Γ_8 states. In particular using the angular momentum addition rule: $\frac{3}{2} \otimes \frac{3}{2} = 3 \oplus 2 \oplus 1 \oplus 0$, we can classify the sixteen possible Cooper pairs as follows:

$J = 0$ singlet state

$$|J=0, m_J=0\rangle = \tfrac{1}{2}\Big(|\tfrac{3}{2}, -\tfrac{3}{2}\rangle - |-\tfrac{3}{2}, \tfrac{3}{2}\rangle - |\tfrac{1}{2}, -\tfrac{1}{2}\rangle + |-\tfrac{1}{2}, \tfrac{1}{2}\rangle\Big); \quad (6)$$

$J = 1$ triplet states

$$|J=1, m_J=1\rangle = \tfrac{1}{\sqrt{10}}\Big(\sqrt{3}|\tfrac{3}{2}, -\tfrac{1}{2}\rangle - 2|\tfrac{1}{2}, \tfrac{1}{2}\rangle + \sqrt{3}|-\tfrac{1}{2}, \tfrac{3}{2}\rangle\Big)$$

$$|J=1, m_J=0\rangle = \tfrac{1}{\sqrt{20}}\Big(3|\tfrac{3}{2}, -\tfrac{3}{2}\rangle - |\tfrac{1}{2}, -\tfrac{1}{2}\rangle - |-\tfrac{1}{2}, \tfrac{1}{2}\rangle + 3|-\tfrac{3}{2}, \tfrac{3}{2}\rangle\Big)$$

$$|J=1, m_J=-1\rangle = \tfrac{1}{\sqrt{10}}\Big(\sqrt{3}|-\tfrac{3}{2}, \tfrac{1}{2}\rangle - 2|-\tfrac{1}{2}, -\tfrac{1}{2}\rangle + \sqrt{3}|\tfrac{1}{2}, -\tfrac{3}{2}\rangle\Big); \quad (7)$$

$J = 2$ quintet states

$$
\begin{aligned}
|J=2, m_J=2\rangle &= \tfrac{1}{\sqrt{2}}\Big(|\tfrac{3}{2},\tfrac{1}{2}\rangle - |\tfrac{1}{2},\tfrac{3}{2}\rangle\Big)\\
|J=2, m_J=1\rangle &= \tfrac{1}{\sqrt{2}}\Big(|\tfrac{3}{2},-\tfrac{1}{2}\rangle - |-\tfrac{1}{2},\tfrac{3}{2}\rangle\Big)\\
|J=2, m_J=0\rangle &= \tfrac{1}{2}\Big(|\tfrac{3}{2},-\tfrac{3}{2}\rangle + |\tfrac{1}{2},-\tfrac{1}{2}\rangle - |\tfrac{1}{2},-\tfrac{1}{2}\rangle - |-\tfrac{3}{2},\tfrac{3}{2}\rangle\Big)\\
|J=2, m_J=-1\rangle &= \tfrac{1}{\sqrt{2}}\Big(|-\tfrac{3}{2},\tfrac{1}{2}\rangle - |\tfrac{1}{2},-\tfrac{3}{2}\rangle\Big)\\
|J=2, m_J=-2\rangle &= \tfrac{1}{\sqrt{2}}\Big(|-\tfrac{3}{2},-\tfrac{1}{2}\rangle - |-\tfrac{1}{2},-\tfrac{3}{2}\rangle\Big);
\end{aligned}
\tag{8}
$$

and $J = 3$ septet states

$$
\begin{aligned}
|J=3, m_J=3\rangle &= |\tfrac{3}{2},\tfrac{3}{2}\rangle\\
|J=3, m_J=2\rangle &= \tfrac{1}{\sqrt{2}}\Big(|\tfrac{3}{2},\tfrac{1}{2}\rangle + |\tfrac{1}{2},\tfrac{3}{2}\rangle\Big)\\
|J=3, m_J=1\rangle &= \tfrac{1}{\sqrt{5}}\Big(|\tfrac{3}{2},-\tfrac{1}{2}\rangle + \sqrt{3}|\tfrac{1}{2},\tfrac{1}{2}\rangle + |-\tfrac{1}{2},\tfrac{3}{2}\rangle\Big)\\
|J=3, m_J=0\rangle &= \tfrac{1}{\sqrt{20}}\Big(|\tfrac{3}{2},-\tfrac{3}{2}\rangle + 3|\tfrac{1}{2},-\tfrac{1}{2}\rangle + 3|-\tfrac{1}{2},\tfrac{1}{2}\rangle + |-\tfrac{3}{2},\tfrac{3}{2}\rangle\Big)\\
|J=3, m_J=-1\rangle &= \tfrac{1}{\sqrt{5}}\Big(|\tfrac{3}{2},-\tfrac{1}{2}\rangle + \sqrt{3}|-\tfrac{1}{2},-\tfrac{1}{2}\rangle + |\tfrac{1}{2},-\tfrac{3}{2}\rangle\Big)\\
|J=3, m_J=-2\rangle &= \tfrac{1}{\sqrt{2}}\Big(|-\tfrac{3}{2},-\tfrac{1}{2}\rangle + |-\tfrac{1}{2},-\tfrac{3}{2}\rangle\Big)\\
|J=3, m_J=-3\rangle &= |-\tfrac{3}{2},-\tfrac{3}{2}\rangle.
\end{aligned}
\tag{9}
$$

Electronic structure and k · p model

Figure 5 presents the band structure of YPtBi. The calculated band structure of YPtBi shown in panel (a) was obtained using the WIEN2K [43] implementation of the full potential linearized augmented plane wave method with the Tran-Blaha modified Becke-Johnson exchange-correlation potential (MBJLDA) [44], with spin-orbital coupling included in the calculation. The k-point mesh was taken to be 11×11×11, and cubic lattice constant a = 664.0(1) pm was obtained from Ref. [34]. The s-like band Γ_6 lies below the p-like band Γ_8, reflecting the nontrivial topology, consistent with previous calculations [31, 32]. Note the splittings will disappear in a non-relativistic calculation, and also it is common to have these spin splittings vanish at high symmetry points and along high symmetry directions. This is because there are symmetry elements that require band degeneracies, which are removed when we move away from these special points. This splitting evidences a j=3/2 analogue of antisymmetric spin-orbit coupling due to broken inversion symmetry, similar to Rashba spin-orbit coupling in tetragonal systems [33].

Figure 5(b) shows ARPES results done on Bi-terminated (111) surface. Numerous bands are observed to cross the Fermi-level ($E_{\rm F}$) from the zone boundary to normal emission. Consistent with ARPES measurements of LuPtBi and GdPtBi [45], the photon energy dependence of most of these bands follows strong vertical streaks along k_z indicative of 2D surface states. Theoretical slab calculations [45] have determined that the surface states, labeled s in Fig. 5(b), originate from a Bi-terminated (111) cleavage plane, and that they are of non-topological origin owing to an even number of $E_{\rm F}$-crossings with the surface Brillouin zone. Aging of the surface in a poorer storage vacuum for a week is observed to suppress all the surface states and leave a single fuzzy broad hole-band feature that reaches to $E_{\rm F}$. A similar inner-hole band pocket was also observed as a single-band with weak intensity in LuPtBi and GdPtBi [45] and assumed to be a pair of nearly degenerate bands from comparison to their slab calculations.

A characteristic Rashba-like splitting of two hole bands is shown in Fig. 5(b) at ≈ 0.5 eV binding energy which also appear in bulk band structure calculations, but at an energy of ≈ -0.8 eV below $E_{\rm F}$. Shifting the theory Γ-L bands to higher energy by ≈ 0.3 eV to align to the Rashba-like split bulk bands, as shown in overplotted dashed lines, causes two other nearly-degenerate hole-like bulk bands that originally just touch $E_{\rm F}$ at a semimetal point, to form a hole-pocket. This large 0.3 eV chemical potential shift in the ARPES measurement, relative to the theory calculation, reflects a possible charge imbalance at the cleaved surface and resultant band bending relative to the bulk.

The experimental quantum oscillation frequency of F = 45 T [7] corresponds to a cross sectional area of a hypothetical spherical Fermi surface $A_F \approx 0.43$

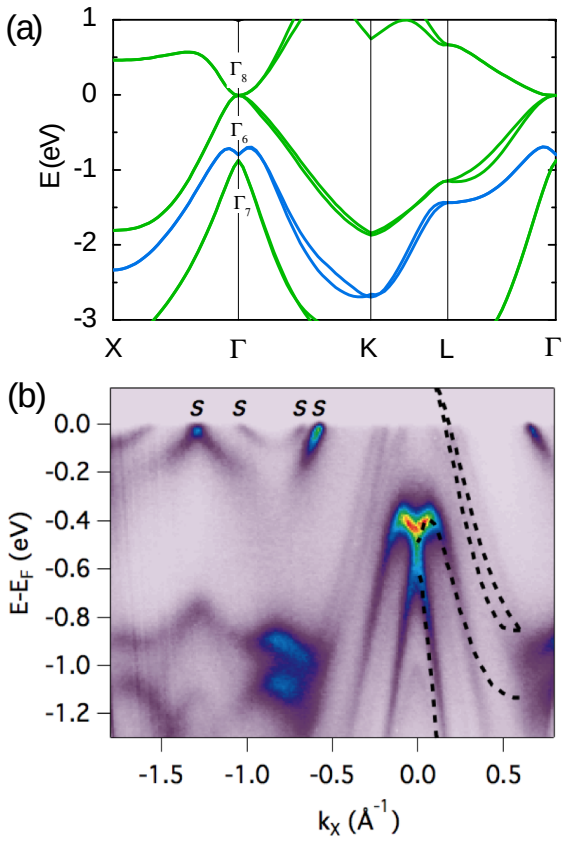

FIG. 5. (a) Calculated band structure of YPtBi obtained using the full potential linearized augmented plane wave method with the Tran-Blaha modified Becke-Johnson exchange-correlation potential (MBJLDA). (b) Results of angle-dependent photoemission spectroscopy (ARPES) measurement done on Bi-terminated (111) surface. The black dashed lines represent the calculated band structure along Γ-L. The chemical potential in ARPES result is about 0.32 eV below that of theoretical result (see Fig. 2 in the main text).

nm^{-2} and a $k_{\rm F}$≈0.037 Å^{-1}, using the Onsager relation $F = \phi_0 A_F/2\pi^2$ where $A_F = \pi k_F^2$ and $\phi_0 = 2.07\times10^{-7}$ G cm^{-2}, which is much smaller than the ARPES $k_{\rm F}$ values in Fig. 2(c) of ≈ 0.1 Å^{-1}. This supports the scenario of a charge imbalance at the surface and band bending with the bulk chemical potential only ≈10 meV below the hole-band maximum.

We treat the antisymmetric spin-orbit coupling (ASOC) as a perturbation of the Luttinger-Kohn model, which has doubly-degenerate eigenenergies

$$\epsilon_{\mathbf{k},\pm} = \left(\alpha + \frac{5}{4}\beta\right)|\mathbf{k}|^2 \pm \beta\sqrt{\sum_i \left[k_i^4 + \left(\tfrac{3\gamma^2}{\beta^2} - 1\right)k_i^2 k_{i+1}^2\right]}. \tag{10}$$

Due to the presence of time-reversal and inversion symmetry for $\delta = 0$, the eigenstates can be labelled by a pseudospin-1/2 index. Proceeding via degenerate perturbation theory, we now include the ASOC by projecting it into the pseudospin basis for each band, hence obtaining two effective pseudospin-1/2 Hamiltonians

$$H_{\rm eff,\pm} = \epsilon_{\mathbf{k},\pm}\hat{s}_0 + \mathbf{g}_{\mathbf{k},\pm}\cdot\hat{\mathbf{s}} \tag{11}$$

where $\hat{s}_\mu$ are the Pauli matrices for the pseudospin, and the vector $\mathbf{g}_{\mathbf{k},\pm} = -\mathbf{g}_{-\mathbf{k},\pm}$ represents the effective ASOC in the pseudospin-1/2 basis of the band $\epsilon_{\mathbf{k},\pm}$. The expression for $\mathbf{g}_{\mathbf{k},\pm}$ is complicated and depends upon the choice of pseudospin basis; an analytic expression for $|\mathbf{g}_{\mathbf{k},\pm}|$ is given elsewhere [19]. The effective pseudospin-1/2 Hamiltonians can be diagonalized by going over to the helicity basis, yielding dispersions $E_{\mathbf{k},\eta=\pm,\nu=\pm} = \epsilon_{\mathbf{k},\eta} + \nu|\mathbf{g}_{\mathbf{k},\eta}|$, where the values of η and ν are independent of one another. In particular, the two spin-split Fermi surfaces are labelled by opposite values of ν. This approximation is in excellent agreement with the exact solutions of the $\mathbf{k}\cdot\mathbf{p}$ for small antisymmetric SOC.

In weak-coupling Bogoliubov-de Gennes theory the pairing is modelled by a term in the Hamiltonian of the form

$$H_{\rm pair} = \sum_{\mathbf{k}}\sum_{j,j'=-3/2}^{3/2}\left\{\Delta_{j,j'}(\mathbf{k})c^\dagger_{\mathbf{k},j}c^\dagger_{-\mathbf{k},j'} + \text{H.c.}\right\}. \tag{12}$$

We restrict our attention to gaps in the A_1 irreducible representation of the T_d point group (i.e. with the full symmetry of the lattice). Allowing pairing in at most a relative p-wave (assuming quasi-local interactions are responsible for the superconductivity, higher-order momentum-dependence is unlikely [46]), we have the general gap

$$\check{\Delta}(\mathbf{k}) = \Delta_s\begin{pmatrix} 0 & 0 & 0 & 1\\ 0 & 0 & -1 & 0\\ 0 & 1 & 0 & 0\\ -1 & 0 & 0 & 0\end{pmatrix} + \Delta_p\begin{pmatrix} \frac{3}{4}k_- & \frac{\sqrt{3}}{2}k_z & \frac{\sqrt{3}}{4}k_+ & 0\\ \frac{\sqrt{3}}{2}k_z & \frac{3}{4}k_+ & 0 & -\frac{\sqrt{3}}{4}k_-\\ \frac{\sqrt{3}}{4}k_+ & 0 & -\frac{3}{4}k_- & \frac{\sqrt{3}}{2}k_z\\ 0 & -\frac{\sqrt{3}}{4}k_- & \frac{\sqrt{3}}{2}k_z & -\frac{3}{4}k_+\end{pmatrix} \tag{13}$$

where $k_\pm = k_x \pm ik_y$. This constitutes a mixed state involving s-wave singlet pairing with strength Δ_s and p-wave *septet* pairing with strength Δ_p. The gap near the Fermi energy can be found by projecting Eq. 13 into the

effective pseudospin-1/2 bands, yielding

$$\Delta_{\text{eff},\pm} = [\Delta_s + (\Delta_p/\delta)(\mathbf{g}_{\mathbf{k},\pm} \cdot \hat{\mathbf{s}})]\, i\hat{s}_y\,. \tag{14}$$

This describes a mixture of pseudospin-singlet and pseudospin-triplet pairing. Importantly, the **d**-vector of the effective pseudospin-triplet pairing is parallel to the ASOC vector $\mathbf{g}_{\mathbf{k},\pm}$. As pointed out by Frigeri *et al.* [15], this alignment makes the pseudospin-triplet component immune to the pair-breaking effect of the ASOC; for sufficiently large ASOC, it is the only stable odd-parity gap. If the singlet state is subdominant, the resulting gap displays line nodes on one of the spin-split Fermi surfaces.

Although the nodal gap prevents us from defining a global topological invariant, the nodal lines themselves represent a nontrivial topological defect in the Brillouin zone. Specifically, the Bogoliubov-de Gennes Hamiltonian $H_{BdG}(\mathbf{k})$ belongs to Altland-Zirnbauer class DIII, which implies that it can be brought into off-diagonal form. This allows us to define the winding number

$$W_{\mathcal{L}} = \frac{1}{2\pi}\mathrm{Im}\oint_{\mathcal{L}} dl \mathrm{Tr}\left\{\nabla_l \ln(D_{\mathbf{k}})\right\} \tag{15}$$

where $D_{\mathbf{k}}$ is the upper off-diagonal block of the Hamiltonian [14, 47, 48]. The winding number $W_{\mathcal{L}}$ takes an integer value along any closed path $\mathcal{L}$ in the Brillouin zone that does not intersect a gap node. Moreover, it is only nonzero if the path $\mathcal{L}$ encircles a line node, defining the topological charge of the node which in our case evaluates to ± 1. This topological charge ensures the existence of a nondegenerate zero-energy surface flat band within the projection of the line node in the surface Brillouin zone [14, 47, 48].

Some alternatives to the mixed singlet-septet state proposed here should be noted. In particular, for purely local pairing interactions, there are five additional s-wave states with quintet total angular momentum [19]. Within a weak-coupling theory, these combine to give time-reversal symmetry-breaking states gaps with Weyl point nodes, and in some cases also line nodes. While such pairing states also topological, they do not yield robust zero-energy surface flat bands [49].

Fig. 6 shows distribution of gap amplitudes $\Delta_k/\max(|\Delta_k|)$ along high symmetry points on the spin-split Fermi surfaces of YPtBi, with a full gap on the outer Fermi surface and gap with line nodes on the inner Fermi surface (see Fig. 4 in the main text). Whereas the fully gapped branch (red) contributes only thermally activated quasiparticles at low temperatures, the line-node branch (blue) manifests a linear temperature variation of the London penetration depth $\Delta\lambda \propto T$, consistent with experimental observations in YPtBi.

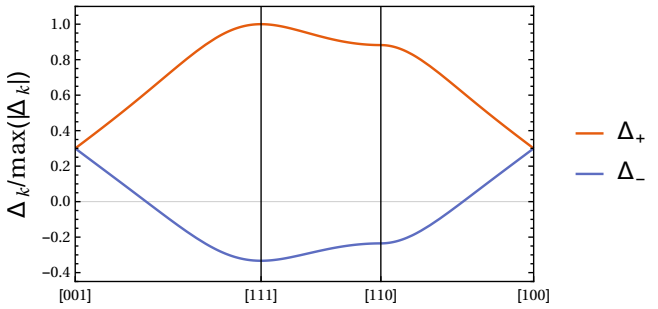

FIG. 6. Normalized magnitude of each gap $\Delta_k/\max(|\Delta_k|)$ along high symmetry points are presented for full gap and nodal gap in red and blue, respectively. Whereas the fully gapped branch (red) contributes only thermally activated quasiparticles at low temperatures, the line-node branch (blue) manifests a linear temperature variation of the London penetration depth $\Delta\lambda \propto T$, consistent with experimental observations in YPtBi.

London penetration depth

The temperature variation of London penetration depth is intimately related to the superconducting order parameter Δ. Within a weak coupling Eilenberger quasiclassical formulation with the perturbation theory of a weak magnetic field [35],

$$(\lambda^2)^{-1}_{ik} = \frac{16\pi^2 e^2 T}{c^2} N(0) \sum_{\omega} \left\langle \frac{\Delta^2 v_i v_k}{(\Delta^2 + \hbar^2\omega^2)^{3/2}} \right\rangle \tag{16}$$

where $N(0)$ is the total density of states at Fermi level per spin, v is the Fermi velocity, and ω is the Matsubara frequency. Measurement of the London penetration depth utilizes a small excitation field $H_{ac} < 2\mu$T, so the Eq. (16) is valid in absence of H_{dc}.

In an s-wave superconductor, an exponential behavior of $\Delta\lambda(T)/\lambda(0) = \sqrt{\pi\Delta_0/2k_BT}\exp(-\Delta_0/k_BT)$ can be deduced from Eq. (16) for a constant gap $\Delta = \Delta_0$, while in a d-wave superconductor $\Delta\lambda(T)$ varies linearly with temperature as $\Delta\lambda(T) = \frac{2\lambda(0)\ln 2}{\mu\Delta_0}T$, at sufficiently low temperatures in a clean sample [36]. Here, μ is the angular slope parameter near the node, *e.g.*, $\mu = 2$ for a d-wave gap $\Delta = \Delta_0(k_x^2 - k_y^2)$. To compare the experimental result for YPtBi to the d-wave gap expectation, one can fix the temperature power of $\Delta\lambda(T)$ to $n = 1$ and obtain a slope prefactor $A = 1.5$ μm/K from fitting, yielding $2\Delta_0/k_BT_c \approx 4/\mu$. Fixing $\mu = 2$ for the d-wave case gives $2\Delta_0 \approx 2k_BT_c$, which is slightly smaller than the weak-coupling BCS value of $2\Delta_0 = 3.52k_BT_c$, and significantly smaller than the observed value for YPtBi observed in STM [26] and point contact measurements (see below).

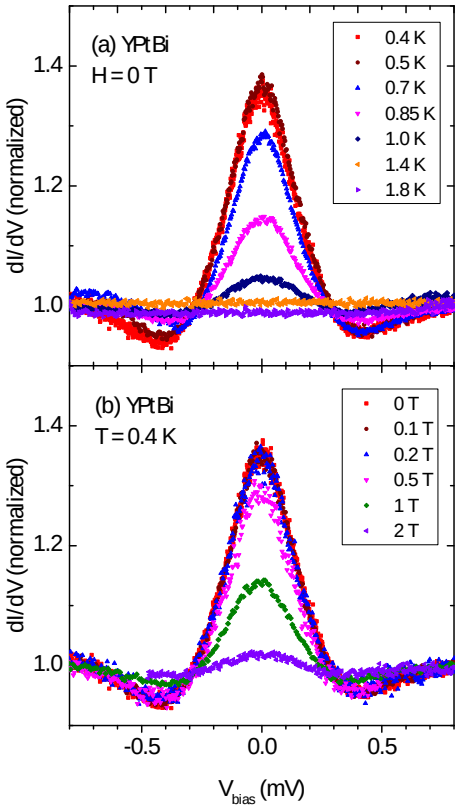

FIG. 7. Soft point-contact spectroscopy conductance spectra of YPtBi as a function of (a) temperature and (b) magnetic field. An enhancement of roughly 40% is observed at zero bias for 0.4 K base temperature in zero field. Note the persistence of the conductance peak associated with the superconducting gap to temperatures above $T_c = 0.78$ K, which may have a relation to the associated theory of $j = 3/2$ pairing [19].

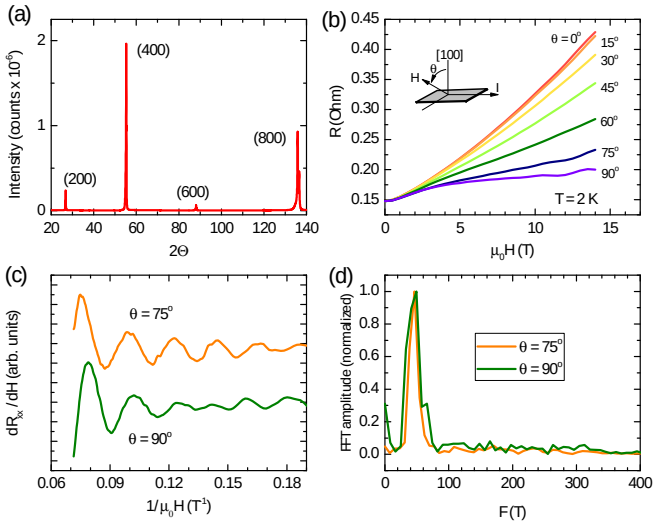

FIG. 8. (a) Single crystal x-ray diffraction pattern of (100) surface of YPtBi. (b) Angle-dependent transverse magnetoresistance R_{xx} at polar angles defined from the crystallographic [100] direction. (b) Comparison of $\theta = 75°$ and 90° oscillatory component plotted as a function of inverse field $(1/\mu_0 H)$. The beating pattern node is readily visible in 90° data near ~ 0.14 T^{-1}, similarly to previous work [7], but moves out of visible range in the 75° data. This observation at higher angles confirms the angle-and field-dependent node shifting found in lower angle data (see Fig. 3(a) in the main text). (c) FFT of dR_{xx}/dH for $\theta = 75°$ and 90°. In both angles, application of FFT results in a broad peak centered at about 49 T. The full width at half maximum is about 30 T for both angles, so the beating frequencies are not discernible in this data set. Nevertheless, nearly angle-independent SdH frequency strongly supports the theoretical Fermi surfaces in Fig. 3(c) in the main text.

Soft point-contact spectroscopy

Point contact spectroscopy was performed using the "soft" point contact technique, with conductance spectra measured on a polished surface of single crystal YPtBi. Contact junctions were prepared by attaching a bent 25 μm gold wire to a sample using DuPont 4929N silver paste. Typical junctions were on the order of 0.1 μm in diameter achieved by pre-coating the surface with a thin layer of stycast with a small hole. dI/dV spectra were measured in a commercial ^{3}He cryostat. AC conductivity vs. DC bias voltage was measured in zero magnetic field at several temperatures between 400 mK and 1.8 K and at multiple applied magnetic fields at 400 mK.

Figure 7 shows the results from point-contact spectroscopy measurements on a single crystal YPtBi. The spectra show strong temperature-and field-dependence on the temperature-and field-independent flat background conductance at high bias as shown respectively in Fig 7(a) and (b). Thus, the observed shape of spectra represents the superconducting gap. The data in Fig. 7 were normalized by dividing by the high bias value for dI/dV. It is notable that dI/dV increases monotonically up to $V_{bias} = 0$. In addition to the shape of the curves, other aspects of the data are also unusual compared to what is expected for conventional superconductivity. First, the zero bias enhancement shown in Fig. 7 persists at values of temperature and magnetic field that are above the values of T_c and H_{c2} that were determined from the resistivity measurements [7, 23]. Second, the size of these gap features is also quite large compared to the expected BCS gap value of $\Delta_0 = 1.76 k_B T_c = 0.1$ meV for a T_c of 0.7 K. In fact, based on the peak width the gap size appears to be at least twice the BCS value. This large deviation from the BCS theory provides further evidence against the conventional s-wave model.

Angle-dependent magnetoresistance

To verify the presence of nearly spherical spin-split bulk Fermi surfaces we studied the angle-dependent Shubnikov-de Haas (SdH) effect. To measure angular

dependence of transverse magnetoresistance (MR), we chose polar angles from crystallographic [100] direction, which was verified by a single crystal x-ray diffraction experiment, shown in Fig. 8(a). Field-dependent MR data in various polar angles are shown in Fig. 8(b). 0° data show almost 200% increased MR at 14 T compared to the resistance in the absence of a magnetic field. SdH oscillations are imposed on smoothly changing MR.

Data obtained at small angles up to $\theta = 25°$ away from the [100] direction reveal a field-dependent node that moves monotonically towards higher field, starting from 12 T at 0°(see Fig. 3(a) in the main text). The shape of oscillation near the node is symmetric about $\theta = 0°$ [100], indicating the node pattern is based on the crystal symmetry. A node in the oscillation is a hallmark of superposition of two similar oscillations, which is often observed in a corrugated 2D Fermi surface [50–52] and also in the spin-split Fermi surfaces as a result of the antisymmetric spin-orbit coupling [53, 54]. In this case, the quantum oscillation is arising from the bulk Fermi surface which is supported by strong oscillations with field along the measured plane ($\theta = 90°$) as well as 75° data as shown in Fig. 8(c). We performed FFT on the first derivative of these two angles as a function of $1/\mu_0 H$, and the resultant frequencies are nearly the same ($F = 49$ T) shown in Fig. 8(d), which supports a nearly spherical Fermi surface.

* hyunsoo@umd.edu
† paglione@umd.edu

[1] M. Z. Hasan and C. L. Kane, Rev. Mod. Phys. **82**, 3045 (2010).
[2] X.-L. Qi and S.-C. Zhang, Rev. Mod. Phys. **83**, 1057 (2011).
[3] S. Chadov, X. Qi, J. Kbler, G. H. Fecher, C. Felser, and S. C. Zhang, Nat Mater **9**, 541 (2010).
[4] H. Lin, L. A. Wray, Y. Xia, S. Xu, S. Jia, R. J. Cava, A. Bansil, and M. Z. Hasan, Nat Mater **9**, 546 (2010).
[5] D. Xiao, Y. Yao, W. Feng, J. Wen, W. Zhu, X.-Q. Chen, G. M. Stocks, and Z. Zhang, Phys. Rev. Lett. **105**, 096404 (2010).
[6] G. Goll, M. Marz, A. Hamann, T. Tomanic, K. Grube, T. Yoshino, and T. Takabatake, Physica B: Condensed Matter **403**, 1065 (2008), proceedings of the International Conference on Strongly Correlated Electron Systems.
[7] N. P. Butch, P. Syers, K. Kirshenbaum, A. P. Hope, and J. Paglione, Phys. Rev. B **84**, 220504 (2011).
[8] F. F. Tafti, T. Fujii, A. Juneau-Fecteau, S. René de Cotret, N. Doiron-Leyraud, A. Asamitsu, and L. Taillefer, Phys. Rev. B **87**, 184504 (2013).
[9] B. Yan and A. de Visser, MRS Bulletin **39**, 859 (2014).
[10] Y. Pan, Nikitin, A. M., Bay, T. V., Huang, Y. K., Paulsen, C., Yan, B. H., and de Visser, A., EPL **104**, 27001 (2013).
[11] Y. Nakajima, R. Hu, K. Kirshenbaum, A. Hughes, P. Syers, X. Wang, K. Wang, R. Wang, S. R. Saha, D. Pratt, J. W. Lynn, and J. Paglione, Science Advances **1** (2015).
[12] R. S. K. Mong, A. M. Essin, and J. E. Moore, Phys. Rev. B **81**, 245209 (2010).
[13] L. Fu, Phys. Rev. B **90**, 100509 (2014).
[14] A. P. Schnyder and P. M. R. Brydon, Journal of Physics: Condensed Matter **27**, 243201 (2015).
[15] P. A. Frigeri, D. F. Agterberg, A. Koga, and M. Sigrist, Phys. Rev. Lett. **92**, 097001 (2004).
[16] E. Bauer and M. Sigrist, *Non-centrosymmetric superconductors: introduction and overview*, Vol. 847 (Springer Science & Business Media, 2012).
[17] T.-L. Ho and S. Yip, Phys. Rev. Lett. **82**, 247 (1999).
[18] W. Yang, Y. Li, and C. Wu, Phys. Rev. Lett. **117**, 075301 (2016).
[19] P. M. R. Brydon, L. Wang, M. Weinert, and D. F. Agterberg, Phys. Rev. Lett. **116**, 177001 (2016).
[20] P. G. Pagliuso, C. Rettori, M. E. Torelli, G. B. Martins, Z. Fisk, J. L. Sarrao, M. F. Hundley, and S. B. Oseroff, Phys. Rev. B **60**, 4176 (1999).
[21] X. Lin, Z. Zhu, B. Fauqué, and K. Behnia, Phys. Rev. X **3**, 021002 (2013).
[22] M. Meinert, Phys. Rev. Lett. **116**, 137001 (2016).
[23] T. V. Bay, T. Naka, Y. K. Huang, and A. de Visser, Phys. Rev. B **86**, 064515 (2012).
[24] T. V. Bay, T. Naka, Y. K. Huang, H. Luigjes, M. S. Golden, and A. de Visser, Phys. Rev. Lett. **108**, 057001 (2012).
[25] K. Kirshenbaum, P. S. Syers, A. P. Hope, N. P. Butch, J. R. Jeffries, S. T. Weir, J. J. Hamlin, M. B. Maple, Y. K. Vohra, and J. Paglione, Phys. Rev. Lett. **111**, 087001 (2013).
[26] H. Baek, J. Ha, D. Zhang, B. Natarajan, J. P. Winterstein, R. Sharma, R. Hu, K. Wang, S. Ziemak, J. Paglione, Y. Kuk, N. B. Zhitenev, and J. A. Stroscio, Phys. Rev. B **92**, 094510 (2015).
[27] D. Daghero, M. Tortello, G. A. Ummarino, and R. S. Gonnelli, Reports on Progress in Physics **74**, 124509 (2011).
[28] K. Sengupta, H.-J. Kwon, and V. M. Yakovenko, Phys. Rev. B **65**, 104504 (2002).
[29] H. Kim, M. A. Tanatar, Y. Liu, Z. C. Sims, C. Zhang, P. Dai, T. A. Lograsso, and R. Prozorov, Phys. Rev. B **89**, 174519 (2014).
[30] V. K. Anand, H. Kim, M. A. Tanatar, R. Prozorov, and D. C. Johnston, Phys. Rev. B **87**, 224510 (2013).
[31] C. Shi, X. Xi, Z. Hou, X. Zhang, G. Xu, E. Liu, W. Wang, W. Wang, J. Chen, and G. Wu, physica status solidi (b) **252**, 357 (2015).
[32] W. Feng, D. Xiao, Y. Zhang, and Y. Yao, Phys. Rev. B **82**, 235121 (2010).
[33] G. Dresselhaus, Phys. Rev. **100**, 580 (1955).
[34] M. G. Haase, T. Schmidt, C. G. Richter, H. Block, and W. Jeitschko, Journal of Solid State Chemistry **168**, 18 (2002).
[35] R. Prozorov and V. G. Kogan, Reports on Progress in Physics **74**, 124505 (2011).
[36] D. Xu, S. K. Yip, and J. A. Sauls, Phys. Rev. B **51**, 16233 (1995).
[37] W. N. Hardy, D. A. Bonn, D. C. Morgan, R. Liang, and K. Zhang, Phys. Rev. Lett. **70**, 3999 (1993).
[38] I. Bonalde, W. Brämer-Escamilla, and E. Bauer, Phys. Rev. Lett. **94**, 207002 (2005).
[39] H. Q. Yuan, D. F. Agterberg, N. Hayashi, P. Badica,

D. Vandervelde, K. Togano, M. Sigrist, and M. B. Salamon, Phys. Rev. Lett. **97**, 017006 (2006).
[40] P. J. Hirschfeld and N. Goldenfeld, Phys. Rev. B **48**, 4219 (1993).
[41] V. Kozii and L. Fu, Phys. Rev. Lett. **115**, 207002 (2015).
[42] Y. Wang, G. Y. Cho, T. L. Hughes, and E. Fradkin, Phys. Rev. B **93**, 134512 (2016).
[43] K. Schwarz, P. Blaha, and G. Madsen, Computer Physics Communications **147**, 71 (2002), proceedings of the Europhysics Conference on Computational Physics Computational Modeling and Simulation of Complex Systems.
[44] F. Tran and P. Blaha, Phys. Rev. Lett. **102**, 226401 (2009).
[45] C. Liu, Y. Lee, T. Kondo, E. D. Mun, M. Caudle, B. N. Harmon, S. L. Bud'ko, P. C. Canfield, and A. Kaminski, Phys. Rev. B **83**, 205133 (2011).
[46] R. Konno and K. Ueda, Phys. Rev. B **40**, 4329 (1989).
[47] A. P. Schnyder and S. Ryu, Phys. Rev. B **84**, 060504 (2011).
[48] P. M. R. Brydon, A. P. Schnyder, and C. Timm, Phys. Rev. B **84**, 020501 (2011).
[49] S. Kobayashi, Y. Tanaka, and M. Sato, Phys. Rev. B **92**, 214514 (2015).
[50] N. Toyota, T. Sasaki, K. Murata, Y. Honda, M. Tokumoto, H. Bando, N. Kinoshita, H. Anzai, T. Ishiguro, and Y. Muto, Journal of the Physical Society of Japan **57**, 2616 (1988), http://dx.doi.org/10.1143/JPSJ.57.2616.
[51] C. Bergemann, S. R. Julian, A. P. Mackenzie, S. NishiZaki, and Y. Maeno, Phys. Rev. Lett. **84**, 2662 (2000).
[52] S. E. Sebastian, N. Harrison, F. F. Balakirev, M. M. Altarawneh, P. A. Goddard, R. Liang, D. A. Bonn, W. N. Hardy, and G. G. Lonzarich, Nature **511**, 61 (2014).
[53] S. Hashimoto, T. Yasuda, T. Kubo, H. Shishido, T. Ueda, R. Settai, T. D. Matsuda, Y. Haga, H. Harima, and Y. Ōnuki, Journal of Physics: Condensed Matter **16**, L287 (2004).
[54] V. P. Mineev and K. V. Samokhin, Phys. Rev. B **72**, 212504 (2005).